Journal of Power Sources 189 (2009) 950–957

Contents lists available at ScienceDirect

Journal of Power Sources

journal homepage: www.elsevier.com/locate/jpowsour

Performance of a solid oxide fuel cell couple operated via in situ catalytic partial oxidation of *n*-butane

Michio Horiuchi[a,*], Fumimasa Katagiri[a], Jun Yoshiike[a], Shigeaki Suganuma[a], Yasue Tokutake[a], Helmut Kronemayer[b,1], Wolfgang G. Bessler[c]

[a] *Shinko Electric Industries, 38 Kitaowaribe, 381-0014 Nagano, Japan*
[b] *Institut für Verbrennung und Gasdynamik (IVG), Universität Duisburg-Essen, Lotharstrasse 1, 47057 Duisburg, Germany*
[c] *Deutsches Zentrum für Luft- und Raumfahrt (DLR), Institut für Technische Thermodynamik, Pfaffenwaldring 38-40, 70569 Stuttgart, Germany*

ARTICLE INFO

Article history:
Received 7 October 2008
Received in revised form 20 December 2008
Accepted 22 December 2008
Available online 30 December 2008

Keywords:
Solid oxide fuel cell (SOFC)
Direct-flame fuel cell (DFFC)
Catalytic partial oxidation (CPO)
High volumetric power density
Hydrocarbon
Reforming

ABSTRACT

The operation of a pair of anode-to-anode-facing solid oxide fuel cells (SOFCs) via in situ catalytic partial oxidation (CPO) of *n*-butane was investigated. In this simple "no-chamber" setup, butane is partially oxidized by heterogeneous reactions inside the porous anodes, providing processed fuel and the heat required for SOFC operation. The cell couple yielded a power density of up to 270 mW cm^{-2}, and the maximum total power obtained was 1.2 W with cell sizes of 13 mm × 23 mm. The maximum electrical efficiency was 1.3%. High CO concentrations of up to 1000 ppm were detected in the exhaust gas, indicating that the cell couple could not efficiently consume the complete provided fuel. A flame, lit at the exhaust, minimized the carbon monoxide level while having insignificant influence on the cell performance. Thermal insulation of the cell couple improved the output remarkably, showing the strong influence of temperature on cell performance. The two cells had a distance of only 2 mm, suggesting a potential for high volumetric power densities in multi-cell configurations for a self-sustained combined heat and power system.

1. Introduction

The high fuel flexibility is a distinct advantage of the solid oxide fuel cell (SOFC) over other fuel cell types. However, upon direct hydrocarbon operation at the anode without humidification, it is difficult to completely prevent carbonaceous deposition, which deteriorates cell performance [1–4]. Even with humidified fuel, the stable operation window depends on a proper choice of fuel/oxidant ratio, cell polarization, anode material and fuel type [5], resulting in a relatively high complexity and an increased cost. Consequently, direct utilization of hydrocarbons with the conventional dual-chamber SOFC is still under development [5–13]. In some approaches, noble metals such as Pt and Ru were added to the anode to promote the electrode performance and to suppress the coking [11–13].

The single-chamber SOFC (SCFC) setup [14–21] is able to mitigate the carbon formation issue because premixed fuel–air is used in its fueling system. Although its simple structure is advantageous, a highly selective electrode activity towards fuel and oxidant is required because the fuel–oxidant mixture is uniformly applied to both electrodes. Additionally, the fuel/air ratio must be strictly controlled to be out of the explosion range [14]. SCFCs also require some measure to heat the system to initiate cell reaction.

With the recently reported direct-flame type solid oxide fuel cell (DFFC) [22–25], the anode is exposed directly to a flame whereas the cathode breathes ambient air. The fuel-rich flame is used for fuel partial oxidation and supplies the anode with hot H_2/CO-rich gases. Therefore, a high catalytic selectivity between the electrodes is not necessary, and the risk of explosion is avoided. In spite of its inherently limited efficiency due to fuel naturally consumed by combustion, the DFFC is attractive since it represents a self-startable and thermally self-sustained system in a simple "no-chamber" geometry with low cost and high fuel flexibility.

The DFFCs reported so far had a simple planar membrane-electrode assembly with the anode facing to a flame. However, to obtain power at a practical level of hundreds of watts or more with this structure, a cell having an unrealistically large area and a corresponding large flame will be needed. Alternatively, a multi-cell cell geometry in which multiple cells are set in parallel to each other can be considered. In this structure, it will be advantageous to reduce the gap among cells as much as possible to achieve a higher power density. This is however limited by an effect known as flame quenching, that is, the extinction of a flame due to interaction with a solid wall [26–28]. A flame will not burn within a gap between two plane-parallel plates that is smaller than the quenching distance.

* Corresponding author. Tel.: +81 26 263 4605; fax: +81 26 263 3904.
E-mail address: michio_horiuchi@shinko.co.jp (M. Horiuchi).
[1] Present address: BASF SE, D-67056 Ludwigshafen, Germany.

0378-7753/$ – see front matter © 2008 Elsevier B.V. All rights reserved.
doi:10.1016/j.jpowsour.2008.12.100

This phenomenon is generally attributed to the cooling of the reaction zone by the wall and the removal of reactive intermediates by surface deactivation or reaction. The quenching distance for almost all hydrocarbon/air flames is larger than 1 mm; for a stoichiometric *n*-butane/air flame it is around 2.5 mm, further increasing with increasing fuel/air equivalence ratio [27]. In the context of multi-cell DFFCs, this suggests that the distance between two cells should be larger than 2.5 mm when a premixed *n*-butane flame is used as a fuel source. This might become a serious restriction to achieve a high power density.

Instead of using an open flame, fuel partial oxidation is also possible using a heterogeneous catalyst. This process is referred to as catalytic partial oxidation (CPO); it is being widely investigated due its use for the production of synthesis gas from hydrocarbons [29,30]. CPO typically takes place at a noble metal mesh (e.g., platinum) with short contact time. Kendall et al. [32] proposed a pre-reforming ruthenium catalyst that is set at upstream and provides reformed fuel to a SOFC. However, typical SOFC porous electrode materials may also be active towards CPO. In a numerical study of single-chamber SOFCs, Hao and Goodwin [31] showed that hydrocarbon/air mixtures are rapidly converted inside the outer region of a porous Ni-based anode under heat release. The resulting H_2/CO-rich gas mixture is then electrochemically oxidized close to the porous anode/solid electrolyte interface. Thus, when operated with hydrocarbon/air mixtures, the porous anode has two functionalities: first, partial oxidation of the hydrocarbon and second, electrochemical reaction of the CPO products. We may therefore refer to the first process as in situ CPO.

In the present study, we propose to combine the simple "no-chamber" geometry of a DFFC with the in situ CPO operation principle of an SCFC. With this concept, the advantages of the DFFC setup (simplicity, no electrode selectivity required) can be applied within a multi-cell structure in which the cell-to-cell distance is not limited by flame quenching. This potentially provides high volumetric power density. We show investigations of the power generation performance of a cell couple in which the cells are placed parallel to each other as a basic unit of a multi-cell structure.

2. Experimental

2.1. Cell preparation

A green sheet consisting of SDC (samarium doped ceria, $Ce_{0.8}Sm_{0.2}O_{2-\delta}$, NexTech materials) powder was prepared through ball milling and doctor blade processes. The cathode (50 wt% SDC–50 wt% $Sm_{0.5}Sr_{0.5}CoO_{3-\delta}$) and anode (5 wt% Rh_2O_3–30 wt% SDC–65 wt% $Co_{0.1}Ni_{0.9}O$) pastes were screen-printed on respective faces of the SDC green sheet, followed by cutting this sheet into predetermined sizes. The obtained three layered rectangular green cells were then co-fired at 1200 °C for 2 h. Platinum meshes were buried into additional paste layers respectively formed on each electrode, and fired again at 1200 °C for 1 h. For some cells, as an additional catalytic agent, platinum was applied onto the anode surface using a hexachloroplatinate aqueous solution (ca. 0.7 mg cm^{-2}).

No separate reduction process for the anode materials was performed. The anode became electroconductive as soon as in situ CPO was initiated (cf. Section 3.1), suggesting that the reduction was easily promoted by the hot reducing gas atmosphere.

2.2. Experimental setup

A couple of the cells were connected in series so that their anodes were set to face each other with a gap of approximately 2 mm as shown in Fig. 1a and b. Premixed *n*-butane and air in various ratios and inflow rates regulated by mass flow controllers

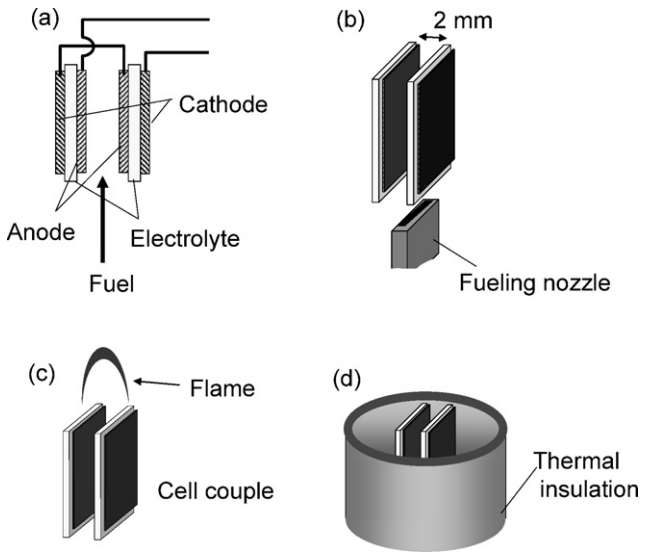

Fig. 1. Experimental setup: (a) Electrical connection of cell couple, (b) base setup operated on in situ catalytic partial oxidation (CPO), (c) setup with flame lit on top of the cell couple, (d) setup with thermal insulation.

were supplied from a thin nozzle (opening 0.5 mm × 10.0 mm, wall thickness: 0.3 mm, nozzle height 6.0 mm). The nozzle was fixed on a *x*–*y*–*z* adjustable fixture for continuous control of the distance between the nozzle top and the cell couple. The air was synthesized from desiccated nitrogen and oxygen, so that the gas mixture was substantially dry. Effects of post-combustion above the cell couple (Fig. 1c) and of thermal insulation (Fig. 1d) on the performance were also investigated.

2.3. Characterization

The performance of the serially connected cells was measured using an electronic load (Chroma ATE Smart Electronic Load 63006). The temperature of the cathode surface was measured optically by infrared pyrometry (NEC-Sanei Corp. Thermotracer TH7102MX). Although an insertion of a thermocouple to the vicinity of the cell couple causes the measured value to be affected, the cell temperature was also determined by a thermocouple when the optical method could not be applied. The carbon monoxide level in the exhaust from the cell couple was monitored by the controlled potential electrolysis method (Testo AG 325 M flue gas analyzer).

3. Results and discussion

3.1. Initiation of in situ catalytic partial oxidation

A flame was lit on the burner nozzle with 400 ml min^{-1} of premixed 6.5% *n*-butane in air about 10 mm under a pair of cells, thus pre-heating the cells. When the burner head was vertically shifted closer to the cell less than ca. 2 mm, the flame extinguished. At the same time, the cells started to glow slightly, and this state continued as long as the premixed gas was supplied. In this operation state, CPO of the fuel takes place spontaneously inside the anodes, sufficiently heating up the cells for electrochemical reactions.

In situ CPO could also be initiated with a flame formed on top of the cell couple. In this case, the nozzle (without flame) was moved directly under the cells, and a flame was lit above the cells (cf. Fig. 1c). Because the gap between the cells was smaller than the flame quenching distance (cf. Section 1), the flame burned stable without flashback. This flame heated the upper parts of the cells to

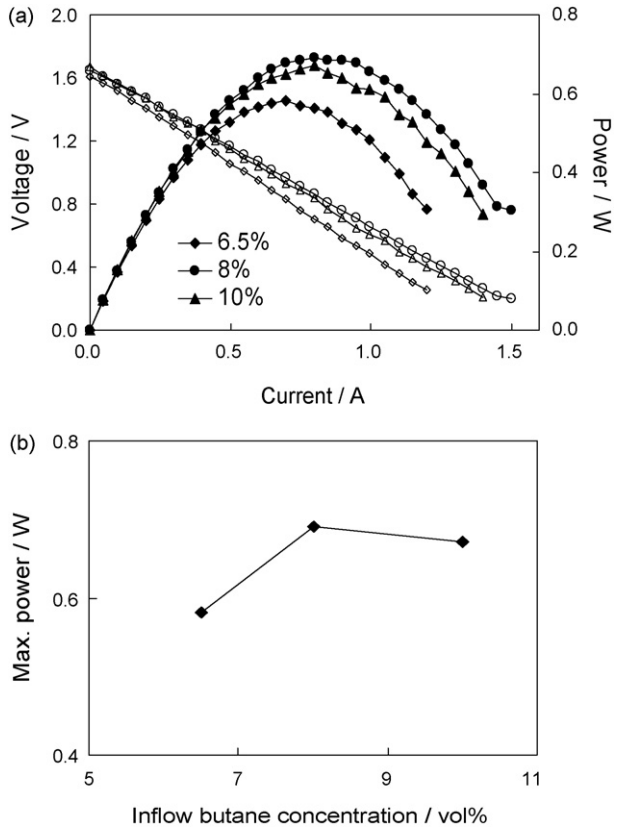

Fig. 2. (a) Polarization curves obtained with 600 ml min^{-1} inflow rate of 6.5%, 8%, 10% *n*-butane/air mixtures, (b) dependence of maximum power on the fuel concentration. Cells without Pt deposition, cell area 10 mm × 13 mm.

red glow; this red area extended gradually to the entire cell area, again indicating CPO activity inside the anode.

CPO activity generally depends on the type and morphology (surface area) of the heterogeneous catalyst [29]. With the present setup, in situ CPO was observed for cells with $Co_{0.1}Ni_{0.9}O$/SDC/Rh_2O_3 anodes both without and with additional platinum deposition. It could not be observed for cells with only a NiO/SDC anode. Note that all anodes included a buried platinum mesh as current collector. These observations show that Rh_2O_3 is sufficiently active as a CPO catalyst. While $Co_{0.1}Ni_{0.9}O$ itself has insufficient CPO activity, it is required as electrocatalyst as well as electron conductor, allowing to transfer electrons to the current collector mesh. Although platinum is known as an excellent CPO catalyst and actually the additional Pt deposition worked notably to enhance CPO, the buried platinum mesh itself does not have a sufficiently large surface area to support CPO. This means that a mesh as a current collector would not need to be made of platinum to promote in situ CPO of the fuel, and hence any other less-expensive metal such as stainless steels will be applicable as an appropriate mesh material.

Note that no visible carbon deposition was observed under all conditions.

3.2. Performance under various fueling conditions

Current–voltage behavior and power densities of 10 mm × 13 mm cells without platinum deposition obtained respectively with 600 ml min^{-1} of 6.5%, 8% and 10% *n*-butane/air are shown in Fig. 2a. The flammability limit of *n*-butane in air is in range of 1.9–8.5%. Therefore, the gas mixtures are within the flammability limit except for 10% *n*-butane/air. However, there is no risk of explosion within the gap between the cells because their distance is below the quenching distance. While no distinctive dependence of OCV (open circuit voltage, approximately 1.6 V) on the fuel concentration was observed, the influence on power output was obvious. A maximum power of 0.7 W was obtained with 8% *n*-butane/air, corresponding to a power density of 270 mW cm^{-2}. The fuel concentration dependence of the maximum power is shown in Fig. 2b. With increasing inflow butane concentration, the output first increased and then slightly decreased again. This tendency is similar to that reported for the direct-flame setup [23], although the equivalence ratio at the peak power in the present study (ϕ = 2.7) differs from that observed with the direct-flame type (ϕ = 1.5). In Ref. [23] it was shown that cell temperature has a dominant influence on both OCV and maximum power. We believe that this is the same case in the present setup, as cell temperature is likely to be influenced by inflow composition.

By a bare flame from a lighter, a large flame could be lit with the effluent gas from the cell couple (cf. Fig. 1c, flame height: 2–5 cm depending on inflow condition), indicating the existence of a large volume of unused fuel. This suggests that the cell area is too small for the amount of fuel supplied. Accordingly, larger cells (13 mm × 23 mm) were prepared. The effect of inflow rate of 8%-premixed *n*-butane/air mixture on the cell output was investigated with the larger cell couple at the same inter-cellular distance as before. As shown in Fig. 3a, OCV decreased with an increase in the inflow rate, likely due to an increase of the cell temperature. A similar trend has also been reported in the direct-flame setup [24], where it was observed that increasing temperature decreases the OCV due to an increase in electronic conductivity of the ceria-based electrolyte (cf. Section 3.4). In the present setup, by using infrared pyrometry, increasing cell temperatures were observed with an increase of the flow rate. The likely reason for this is that a higher flow rate provides more fuel and, therefore, more thermal energy can be released through CPO. This is the case despite the fact that the contact time of the fuel with the catalyst decreases.

With all inflow rate conditions shown in Fig. 3a, a flame could be formed on the cell couple (cf. Fig. 1c), indicating the unburnt fuel residue still remains at a flammable level. The performance characteristics obtained with such a coexisting flame are shown in Fig. 3b. Comparison with Fig. 3a shows that the flame has only a minor influence on the cell performance. The maximum power is plotted versus inflow rate in Fig. 3c. The output increased with an increase in the flow rate of up to approximately 1400 ml min^{-1} where a plateau-like behavior is observed; the maximum power was ca. 1.1 W, corresponding to a power density of 180 mW cm^{-2}. Note that the absolute power is larger than the one obtained with the smaller cells (Fig. 2), however the power density is smaller.

The results shown here show similar trends with regard to fuel concentration and inflow rate as observed previously with the direct-flame type setup [22–25]. Yet, the principle of fuel processing is very different not only due to a difference in flow field (here: fuel flow parallel to the anode, previous work: fuel flow perpendicular the anode) but also due to the existence of a gas volume enclosed from two sides by anode faces. This volume is expected to be enriched with fuel species reformed by the anode surfaces. In the single-chamber type setup, a pair of cells in which anodes face each other has been demonstrated by Shao et al. [18], and most likely a similar phenomenon took place, though both anode and cathode were exposed to the same fuel–air mixture in their system. Shao et al. confirmed that an anode-facing-cathode geometry resulted in almost zero OCV, probably because the active fuel species were rapidly consumed on the cathode surface.

The performance of Pt-deposited cells (13 mm × 23 mm) without and with a flame lit on top of the cell couple is shown in Fig. 4a and b, where the inter-cellular gap was the same as mentioned above. The fuel composition was premixed 8% *n*-butane/air with

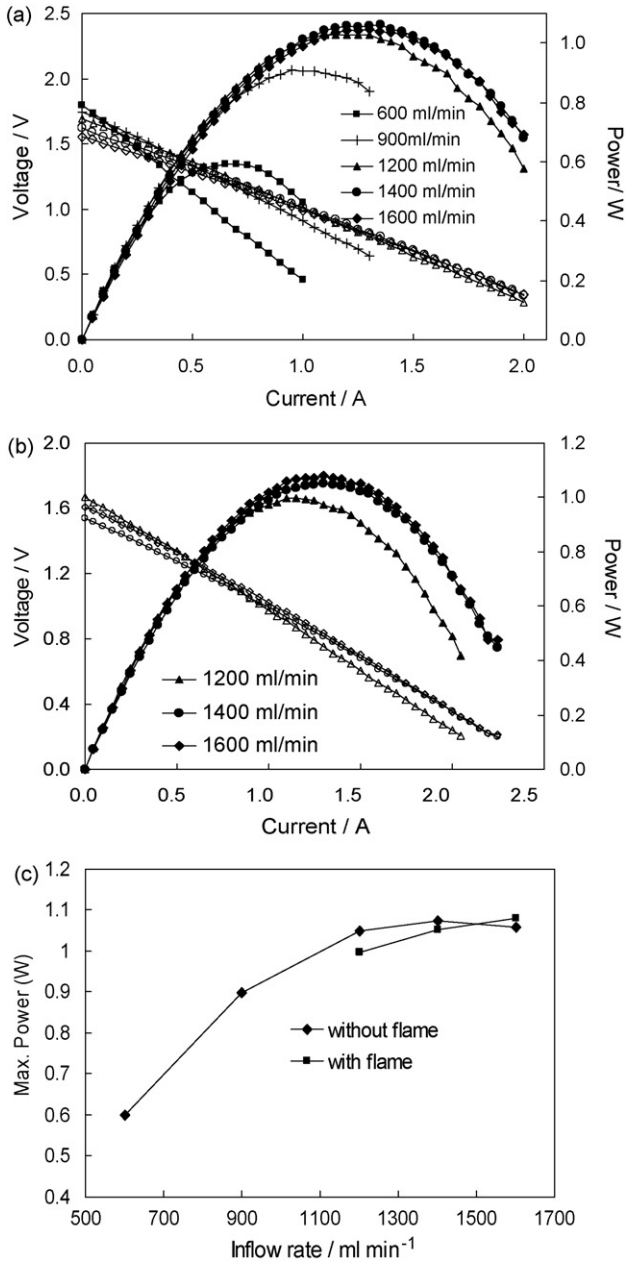

Fig. 3. (a) Polarization curves obtained with 8% *n*-butane/air mixtures at inflow rates between 600 and 1600 ml min^{-1}, (b) polarization curves with a flame lit on the cell couple (Fig. 1c), (c) dependence of the maximum power on the fuel inflow rate. Cells without Pt deposition, cell area 13 mm × 23 mm.

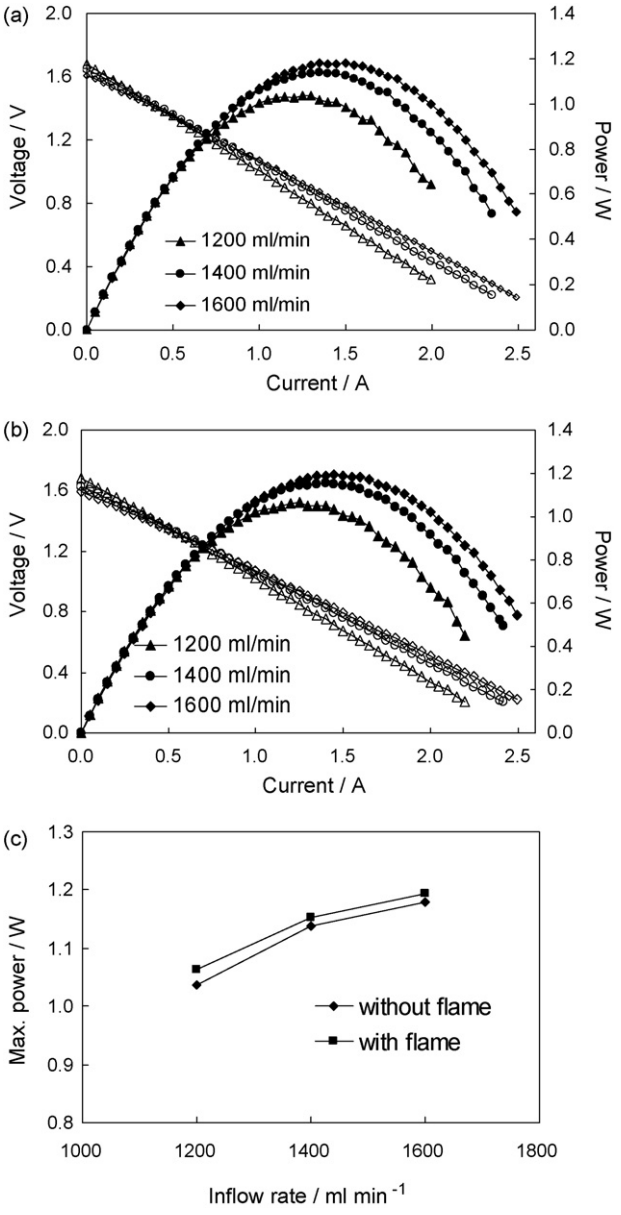

Fig. 4. Polarization curves of the Pt-deposited cells (a) without and (b) with flame lit on the cell couple. (c) Dependence of the maximum power on the fuel inflow rate. Cell area 13 mm × 23 mm.

inflow rates of 1200, 1400, and 1600 ml min^{-1}. The variation of OCV with inflow rate decreased somewhat compared to cells without Pt-deposition. At the same time, maximum power output was increased by around 10%. As shown in Fig. 4c, the dependence of cell performance on inflow rate became more pronounced compared to cells without Pt deposition, a higher inflow rate leading to a higher output. The influence of the flame lit on the cell couple was only weak, however always positive for output, which was not the case for the cells without Pt deposition (Fig. 3c).

3.3. Exhaust CO concentration

The dependence of CO concentration measured in the exhaust of the cell couple on the inflow rate is shown in Fig. 5a for 8% *n*-butane/air mixture supply. This graph is corresponding to Figs. 3a, 3b, 4a, 4b, and the power output was always higher than 1 W. With Pt deposition, CO concentration tends to become higher compared with that without Pt deposition, suggesting the catalytic reforming of *n*-butane was promoted by the deposited Pt. The CO concentration increased with increasing inflow rate for the Pt-deposited cell couple, whereas, without the Pt deposition, the highest concentration (ca. 550 ppm) was detected with the lowest inflow rate (1200 ml min^{-1}) and decreased with an increase in the inflow rate. Although this behavior must be related to the difference in CPO activity, a detailed interpretation is not possible at the present stage. It is likely that cell temperature, which in turn is affected by flow rate and CPO activity, plays an important role.

CO level drastically decreased when a flame was lit on the cell couple, reflecting that CO was fully oxidized in the flame.

With a fixed inflow rate of 1200 ml min^{-1}, the effect of *n*-butane concentration on CO concentration is shown in Fig. 5b, where output obtained under each condition is also given. CO concentration increased linearly while the fuel concentration increased from 6%

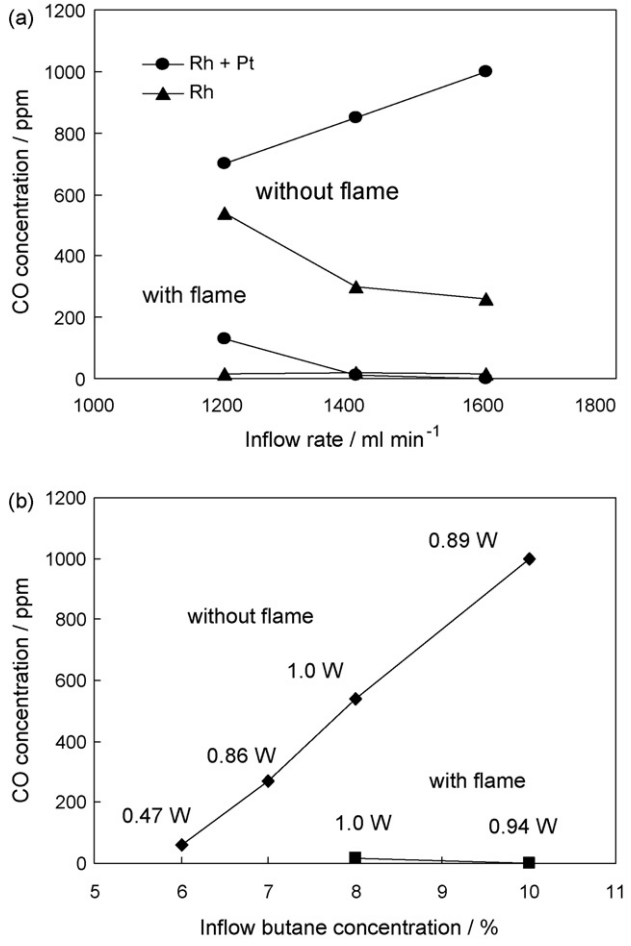

Fig. 5. Correlation between CO concentration detected in exhaust and (a) the inflow rate of 8% *n*-butane–air mixture, (b) the *n*-butane concentration at 1200 ml min^{-1} inflow rate, both with and without a flame lit on the cell couple.

to 10%. The concentration of the other partially oxidized fuel species such as H_2 can be assumed to vary with the same tendency as CO, and accordingly reformed fuel will be richest at the highest supply concentration. Nonetheless, the highest output was observed at intermediate concentrations. This is probably due to both a poor fuel utilization ability and an insufficient effective reaction area (i.e., cell size).

3.4. Temperature distribution and effect of thermal insulation

Fig. 6 shows the typical temperature distribution on a cathode surface of a cell couple generating power. The temperature on a small area close to the fuel inflow was above 800 °C, but as a whole, the cell temperature was in the 600–700 °C range, and not homogeneous.

The effect of thermal insulation on the cell output is shown in Fig. 7a, where the cell couple (13 mm × 23 mm) was thermally insulated within a cylindrically shaped, ca. 2.5 mm thick inorganic woven fabric (cf. Fig. 1d) and fueled with 6% *n*-butane/air. The cell temperature rose over 800 °C (measured by thermocouple), and the uniformity of the temperature was probably improved, though it could not be confirmed by optical thermometry since it was covered. Due to the higher temperature, cell output was remarkably improved especially with low inflow rates. However, Fig. 7b shows that with increasing inflow rate, the cell output first increased to a peak at 600 ml min^{-1} and then decreased again, although the cell temperature is expected to further increase with increasing inflow

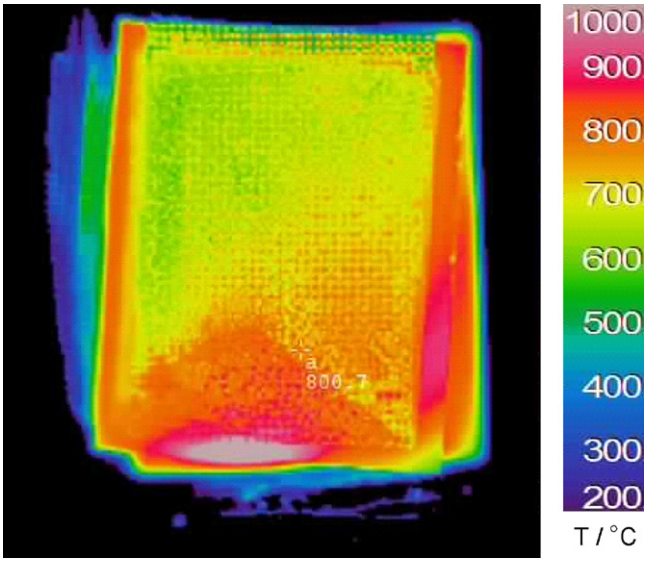

Fig. 6. Temperature distribution on a cathode surface of the cell couple.

rate. These results demonstrate the strong influence of temperature on the cell performance. A similar trend was also observed for similar cells in a direct-flame type setup, where the power output increased with increasing cell temperature up to ~650 °C and then decreased again [23]. This behavior can be interpreted to be caused

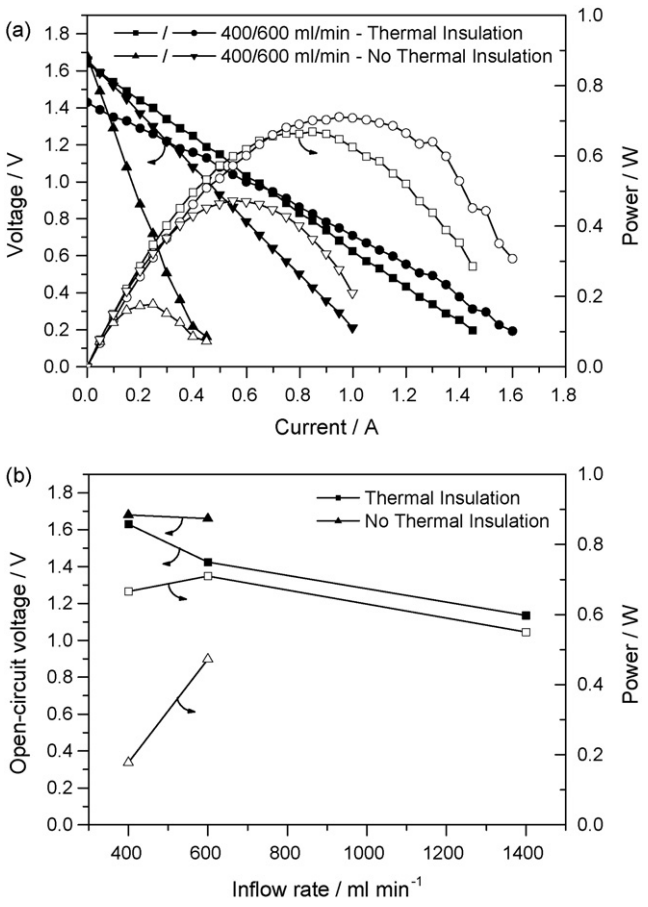

Fig. 7. Effect of thermal insulation on cell performance. (a) Polarization curves with and without thermal insulation. (b) Correlation between fuel inflow rate, OCV and the maximum power. Inflow *n*-butane concentration was 6%. Cell area 13 mm × 23 mm.

by the electronic conductivity of the mixed-conducting SDC electrolyte which is strongly promoted through increasing temperature [33,34]. For a high cell performance, an appropriate thermal management is important in order to keep temperature in an optimum range.

3.5. Electrical efficiency

In this section, various influences on the electrical efficiency of the SOFC/CPO system are analyzed following the approach of Vogler et al. [24]. The total electrical efficiency ε is defined as the ratio of electrical power over heating power of supplied fuel,

$$\varepsilon = \frac{\text{electrical power output of SOFC}}{\text{heating power of supplied fuel}} = \frac{IEV^{\mathrm{M}}}{\dot{V}_{\mathrm{in}} x_{\mathrm{butane}} \mathrm{HHV}_{\mathrm{butane}}}, \quad (1)$$

where I (A) is the current, E (V) the cell voltage, $\dot{V}_{\mathrm{in}}$ ($\mathrm{m^3\,s^{-1}}$) the volumetric inflow rate at standard conditions, x_{butane} the butane mole fraction of the gas inlet, $V^{\mathrm{M}} = 2.24 \times 10^{-2}\,\mathrm{m^3\,mol^{-1}}$ the molar volume at standard conditions, and $\mathrm{HHV}_{\mathrm{butane}} = 2.88 \times 10^{6}\,\mathrm{J\,mol^{-1}}$ [35] the higher heating value of n-butane. The efficiency ε is readily calculated because all terms in Eq. (1) are known for a given operating condition.

For further analysis, the total efficiency can be represented as product of three contributions,

$$\varepsilon = \varepsilon^{\mathrm{cpo}} \varepsilon^{\mathrm{fu}} \varepsilon^{\mathrm{cell}}. \quad (2)$$

In the following, analytical expressions for these contributions are derived based on a number of simplifying assumptions in order to approximate the importance of the various contributions.

3.5.1. Available energy after catalytic partial oxidation ε^{cpo}

During CPO, a part of the fuel's chemical energy is converted to heat, and only a part $\varepsilon^{\mathrm{cpo}}$ is available for operating the fuel cell, where

$$\varepsilon^{\mathrm{cpo}} = \frac{\text{heating power of fuel available for SOFC after CPO}}{\text{heating power of supplied fuel}} \quad (3)$$

In order to estimate an expression for $\varepsilon^{\mathrm{cpo}}$, we hypothetically separate the fuel into a part $n^{\mathrm{ox}}_{\mathrm{butane}}$ that is fully oxidized to CO_2 and H_2O under heat release, and a remaining part whose full heating power is available for the SOFC. This separation is justified by thermodynamics. With this assumption, $\varepsilon^{\mathrm{cpo}}$ is given by

$$\varepsilon^{\mathrm{cpo}} = \frac{n_{\mathrm{butane}} - n^{\mathrm{ox}}_{\mathrm{butane}}}{n_{\mathrm{butane}}}, \quad (4)$$

where n_{butane} is the total inflow rate of butane. We furthermore assume that the partial oxidation reaction rapidly consumes the complete available O_2 (i.e., high catalytic activity). $n^{\mathrm{ox}}_{\mathrm{butane}}$ can then be expressed in terms of the supplied air n_{air} according to the stoichiometry of the butane oxidation reaction (21% O_2 in air)

$$C_4H_{10} + 6.5\,O_2 + 24.45\,N_2 \rightarrow 4\,CO_2 + 5\,H_2O + 24.45\,N_2, \quad (5)$$

from which it follows that $n^{\mathrm{ox}}_{\mathrm{butane}}/n_{\mathrm{air}} = 0.0323$. Substituting into Eq. (4) and using the definition of the fuel mole fraction in the inlet gas $x_{\mathrm{butane}} = n_{\mathrm{butane}}/(n_{\mathrm{butane}} + n_{\mathrm{air}})$ yields the desired relationship

$$\varepsilon^{\mathrm{cpo}} = 1.0323 - 0.0323/x_{\mathrm{butane}}. \quad (6)$$

Eq. (6) shows that the butane mole fraction should be as high as possible for high cell efficiency. Catalytic partial oxidation can realize a higher efficiency ($\varepsilon^{\mathrm{cpo}}$) compared with that of combustion in a flame that is limited by flammable fuel concentration.

3.5.2. Fuel utilization ε^{fu}

Catalytic partial oxidation is a relatively fast process taking place inside the porous anodes. The fuel cell, in contrast, is governed by comparatively slower electrochemical reactions and is typically not able to convert all available partial oxidation products (H_2, CO). Thus, only a part $\varepsilon^{\mathrm{fu}}$ is used electrochemically, where

$$\varepsilon^{\mathrm{fu}} = \frac{\text{heating power of fuel consumed by SOFC}}{\text{heating power of fuel available for SOFC after CPO}} \quad (7)$$

The fuel utilization can be expressed through the molar balance of oxidizer (either O^{2-} in the SOFC or O_2 in gas phase) according to

$$\varepsilon^{\mathrm{fu}} = \frac{\text{oxidizer supplied by SOFC}}{\text{oxidizer needed to complete fuel oxidation after CPO}} = \frac{\text{oxidizer supplied by SOFC}}{\varepsilon^{\mathrm{cpo}}(\text{total oxidizer needed for inlet fuel oxidation})}. \quad (8)$$

Going over to a measure of the oxidizer in electron current yields

$$\varepsilon^{\mathrm{fu}} = \frac{IV^{\mathrm{M}}}{\varepsilon^{\mathrm{cpo}} 4F f_{\mathrm{stoich}} \dot{V}_{\mathrm{in}} x_{\mathrm{butane}}}, \quad (9)$$

where F is Faraday's constant and $f_{\mathrm{stoich}} = 6.5$ is the oxygen/fuel molar ratio for stoichometric butane oxidation.

3.5.3. Cell's electrical efficiency ε^{cell}

The electrical efficiency $\varepsilon^{\mathrm{cell}}$ of the fuel cell is defined here as

$$\varepsilon^{\mathrm{cell}} = \frac{\text{electrical power output of SOFC}}{\text{heating power of fuel consumed by SOFC after CPO}} \quad (10)$$

In theory, the electrical efficiency of a fuel cell is ~90%, given via thermodynamical relationships as the ratio of the free enthalpy over the enthalpy, $\Delta G/\Delta H$. In practice, polarization losses from finite electrochemical kinetics and transport limitations reduce the electrical efficiency. The quantification of $\varepsilon^{\mathrm{cell}}$ is possible via Eq. (2) because the other contributions are known via Eqs. (6) and (9).

In the present work, the highest electrical efficiency was obtained in the setup with thermal insulation (Fig. 7). For the inflow rate of 400 ml $\mathrm{min^{-1}}$, butane concentration of 6% and maximum power of 0.67 W, the total electrical efficiency is $\varepsilon = 1.3\%$. This is a low value, however must be seen in the light of the simplicity of the system and its expected main application for combined heat and power. Furthermore, it is more than twice the efficiency obtained earlier with a direct-flame type setup [24]. The three contributions can be quantified to $\varepsilon^{\mathrm{cpo}} = 49.4\%$, $\varepsilon^{\mathrm{fu}} = 3.6\%$, and $\varepsilon^{\mathrm{cell}} = 73.1\%$. In the catalytic partial oxidation type setup, the efficiency of fuel conversion $\varepsilon^{\mathrm{cpo}}$ is much larger than in the direct-flame setup (~10%) because higher equivalence ratios can be used. The most important contribution to low overall efficiencies is the low utilization of the partial oxidation products by the fuel cell. This is also the reason for the observed high CO concentrations and flammability of the exhaust gases. Fuel utilization could be increased by optimizing the insulation design in order to allow lower inflow rates while still keeping the cell temperature high. Finally, the polarization losses of the cell additionally reduce overall efficiency. The calculated cell efficiency (73.1%) is somewhat higher than what would be expected from the polarization curves at maximum power density (ca. 50% polarization losses); the reason for this discrepancy probably lies in the simplifying assumptions in the above calculations.

3.6. High power per volume density cell modules

Since relatively high area-specific power densities of up to 270 mW $\mathrm{cm^{-2}}$ have been verified with a pair of cells that are separated by a 2 mm gap, multi-cell structures are expected to be able to provide a very high volumetric power density. Such

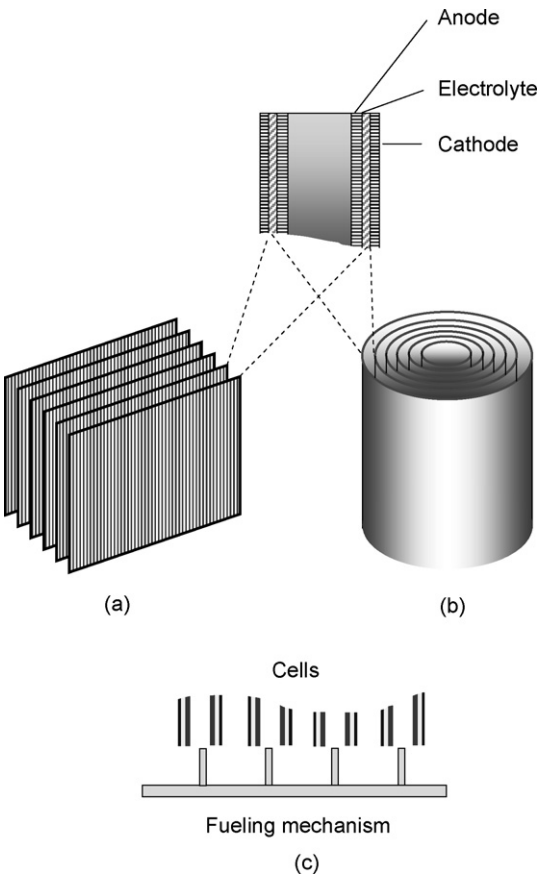

Fig. 8. Schematic structure of multi-cell configurations. (a) Parallel planar type, (b) coaxial cylindrical type cell modules. (c) Fueling mechanism.

structures could be of a planar parallel type or of a coaxial cylindrical type, as illustrated in Fig. 8. While the planar parallel type will be easier to fabricate compared with the coaxial cylindrical type, the latter will be superior in thermal efficiency to the former type. When multiple rectangular cells are set up in a 10 cm × 10 cm × 10 cm space with a 2 mm gap and the obtainable area-specific power density is assumed 200 mW cm^{-2}, an available total power can be estimated as approximately 720 W. It is expected that the cell couple will work sufficiently even with an inter-cellular distance of less than 2 mm, though this was not tested in the present study because the gas supply nozzle was relatively wide.

In practical applications, CO emissions should be minimized to almost zero from a safety viewpoint. The rate of fuel supply will accordingly need to be balanced to the total effective cell area in an optimal thermal management. On the other hand, a good thermal insulation will not always produce the best result due to the influence of the mixed-conducting electrolyte, and fuel utilization efficiency is also limited. For these reasons, lighting and holding a flame in the exhaust might be a solution. This will become a burner or a heater utilizing this excessive heat from the system. This structure is similar to that proposed by Kendall et al. [32], though their SOFC has a single tubular structure. These types of fuel cells with such a heating function will have applications as combined heat and power system.

The present system still has plenty of room for improvements to realize a highly efficient self-sustaining power generation system. To achieve this, optimization of thermal management, application of a stabilized zirconia electrolyte instead of SDC to avoid electronic loss currents, and use of thinner electrolytes in an anode-supported cell structure will be effective approaches.

4. Conclusions

We have investigated the performance of an SOFC couple operated via in situ catalytic partial oxidation of *n*-butane. In this setup, butane is partially oxidized by heterogeneous reactions inside the porous anode, providing processed fuel and the heat required for SOFC operation. Unlike in the direct-flame type setup investigated earlier [22–24], there is no free flame and therefore the geometry of the cell arrangement is not limited by the flame quenching distance. The results of this study are summarized as follows.

- Power densities of up to 270 mW cm^{-2} were observed in a simple and thermally self-sustained "no-chamber" arrangement of two parallel anode-to-anode-facing SOFCs.
- The cell performance varied with fuel composition and inflow rate. A strong influence of temperature on cell performance was observed. By applying a thermal insulation, cell performance could be significantly increased.
- A maximum electrical efficiency of 1.3% (HHV) was obtained. This low value must be seen in the light of the simplicity of the system and its expected main application for combined heat and power.
- High CO emissions of up to 1000 ppm were detected due to the poor fuel utilization. They could be strongly reduced by lighting a flame on top of the cell couple. The flame did not significantly affect cell performance.
- The thin gap between cells (2 mm) verified in the present study will allow a high volumetric power density when applied to multi-cell structures such as a parallel planar cells or coaxial cylindrical cells.

References

[1] C.M. Finnerty, N.J. Coe, R.H. Cunningham, R.M. Ormerod, Catal. Today 46 (1998) 137–145.
[2] S. Assabumrungrat, N. Laosiripojana, V. Pavarajarn, W. Sangtongkitcharoen, A. Tangjitmatee, P. Praserthdam, J. Power Sources 139 (2005) 55–60.
[3] G.K. Gupta, A.M. Dean, K. Ahn, R.J. Gorte, J. Power Sources 158 (2005) 497–503.
[4] S. McIntosh, H. He, S.-I. Lee, O. Cost-Nunes, V.V. Krishnan, J.M. Vohs, R.J. Gorte, J. Electrochem. Soc. 151 (2004) A604–A608.
[5] T. Iida, M. Kawano, T. Matsui, R. Kikuchi, K. Eguchi, J. Electrochem. Soc. 154 (2007) B234–B241.
[6] M. Kawano, T. Matsui, R. Kikuchi, H. Yoshida, T. Inagaki, K. Eguchi, J. Electrochem. Soc. 154 (2007) B460–B465.
[7] T. Kim, G. Liu, M. Boaro, S.I. Lee, J.M. Vohs, R.J. Gorte, O.H. Al-Madhi, B.O. Dabbousi, J. Power Sources 155 (2006) 231–238.
[8] S.P. Jiang, X.J. Chen, S.H. Chan, J.T. Kwok, J. Electrochem. Soc. 153 (2006) A850–A856.
[9] V.M. Janardhanan, O. Deutschmann, J. Power Sources 162 (2006) 1192–1202.
[10] Y. Lin, Z. Zhan, J. Liu, S.A. Barnett, Solid State Ionics 176 (2005) 1827–1835.
[11] K. Zupan, M. Marinsek, S. Pejovnik, K. Pucelj, Mater. Technol. 39 (2005) 163–167.
[12] T. Takeguchi, R. Kikuchi, T. Yano, K. Eguchi, K. Murata, Catal. Today 84 (2003) 217–222.
[13] J.L. Hertz, H.L. Tuller, J. Electrochem. Soc. 154 (2007) B413–B418.
[14] T. Hibino, A. Hashimoto, T. Inoue, J. Tokuno, S. Yoshida, M. Sano, Science 288 (2000) 2031–2033.
[15] T. Suzuki, P. Jasinski, V. Petrovsky, H.U. Anderson, J. Electrochem. Soc. 151 (2004) A1473–A1476.
[16] P. Jasinski, T. Suzuki, F. Dogan, H.U. Anderson, Solid State Ionics 175 (2004) 35–38.
[17] T.W. Napporn, X. Jacques-Bedard, F. Morin, M. Meunier, J. Electrochem. Soc. 151 (2004) A2088–A2094.
[18] Z. Shao, S.M. Haile, J. Ahn, P.D. Rhonny, Z. Zhan, S.A. Barnett, Nature 435 (2005) 795–798.
[19] B.E. Buergler, A.N. Grundy, L.J. Gauckler, J. Electrochem. Soc. 153 (2006) A1378–A1385.
[20] M. Yano, A. Tomita, M. Sano, T. Hibino, Solid State Ionics 177 (2007) 3351–3359.
[21] I. Riess, J. Power Sources 175 (2008) 325–337.
[22] M. Horiuchi, S. Suganuma, M. Watanabe, J. Electrochem. Soc. 151 (2004) A1402–A1405.
[23] H. Kronemayer, D. Barzan, M. Horiuchi, S. Suganuma, Y. Tokutake, C. Schulz, W.G. Bessler, J. Power Sources 166 (2007) 120–126.
[24] M. Vogler, D. Barzan, H. Kronemayer, C. Schulz, M. Horiuchi, S. Suganuma, J. Warnatz, W.G. Bessler, ECS Trans. 7 (2007) 555–564.
[25] K. Wang, R. Ran, Y. Hao, Z. Shao, W. Jin, N. Xu, J. Power Source 177 (2008) 33–39.
[26] J. Warnatz, U. Maas, R.W. Dibble, Combustion, third ed., Springer, Heidelberg, 2001, pp. 208–260.

[27] I. Glassman, Combustion, third ed., Academic Press, San Diego/London/Boston/New York/Sydney/Tokyo/Tronto, 1996, pp. 170–607.
[28] B. Lewis, G. von Elbe, Combustion Flames and Explosions of Gases, third ed., Academic Press, Orland, 1987, pp. 239–380.
[29] R.E. Hayes, S.T. Kolaczkowski, Introduction to Catalytic Combustion, CRC Press, 1997.
[30] R. Quiceno, O. Deutschmann, J. Warnatz, J. Pérez-Ramírez, Catal. Today 119 (2007) 311–316.
[31] Y. Hao, D.G. Goodwin, J. Electrochem. Soc. 155 (2008) B666–B674.
[32] K. Kendall, C.M. Finnerty, J.C. Austin, T. Alston, J. Mater. Sci. 36 (2001) 1119–1124.
[33] M. Godickemeier, L.J. Gauckler, J. Electrochem. Soc. 145 (1998) 414–421.
[34] I. Riess, Solid State Ionics 157 (2003) 1–17.
[35] D.R. Lide (Ed.), CRC Handbook of Chemistry and Physics, 87 ed., CRC Press, Boca Raton, Florida, USA, 2006.